Article

Luminescent Carbon Dot Mimics Assembled on DNA

Ke Min Chan, Wang Xu, Hyukin Kwon, Anna M Kietrys, and Eric T. Kool

J. Am. Chem. Soc., **Just Accepted Manuscript** • DOI: 10.1021/jacs.7b07420 • Publication Date (Web): 25 Aug 2017

Luminescent Carbon Dot Mimics Assembled on DNA

Ke Min Chan, Wang Xu, Hyukin Kwon, Anna M. Kietrys and Eric T. Kool*

Department of Chemistry, Stanford University, Stanford, CA 94305

*to whom correspondence should be addressed: kool@stanford.edu

Abstract. Nanometer-sized fragments of carbon in the form of multilayer graphene ("carbon dots") have been under highly active study for applications in imaging. While offering advantages of low toxicity and photostability, such nanomaterials are inhomogeneous and have limited wavelengths of emission. Here we address these issues by assembling luminescent aromatic C16-C38 hydrocarbons together on a DNA scaffold in homogeneous, soluble molecular compounds. Monomer deoxyribosides of five different aromatic hydrocarbons were synthesized and assembled into a library of 1296 different tetramer compounds on PEG-polystyrene beads. These were screened for photostability and a range of emission colors using 365 nm excitation, observing visible light (>400 nm) emission. We identified a set of six oligomers (carbon dot assemblies, DNA-CAs) with exceptional photostability that emit from 400 to 680 nm in water, with Stokes shifts of up to 110 nm, quantum yields ranging from 0.01 to 0.29, and fluorescence lifetimes from 3 to 42 ns. In addition, several of these DNA-CAs exhibited white emission in aqueous solution. The molecules were used in multispectral cell imaging experiments, and were taken up into cells passively. The results expand the range of emission properties that can be achieved in water with all-hydrocarbon chromophores, and establish the use of the DNA scaffold to arrange carbon layers in homogeneous, rapidly synthesized assemblies.

Introduction

Among the most promising of luminescent materials is carbon in its graphite allotrope.[1-2] Single layers of graphite (graphene) have extremely interesting electronic properties,[3] and fragments of graphene consisting of one to a few layers, ~1-20 nm in size, have been studied intensely over the past decade.[4] Small nanofragments of graphitic carbon, known as carbon dots (CD), or graphene quantum dots (GQD), exhibit many of the electronic properties of semiconductor quantum dots (QD), such as quantum confinement effects, while enjoying the benefit of reduced toxicity by virtue of being free from heavy metals contained in semiconductor materials.[5] Carbon dots display broad UV absorption, and commonly emit in blue and green wavelengths, and occasionally further to the red.[5] They have been functionalized via oxidation, which has allowed them to be conjugated to proteins and to DNA.[6-7] The possibility of using low-toxicity carbon as the basis of luminescent quantum dots is appealing for biological applications, and is one of the strongest motivators in the graphene research field.[8]

A significant limitation of single-layer and few-layer graphene quantum dots is their inhomogeneity. They are challenging to synthesize and manipulate in a reproducible way, hindering both basic study and applications.[9] The source of undesired inhomogeneity arises from the synthetic approaches used in fabricating carbon dots, which fall into two general categories, “bottom-up” and “top-down”.[5] In top-down approaches, carbon dots are typically prepared by breaking down bulk carbon sources, such as graphite, carbon soot, and carbon nanotubes, via destructive methods such as arc discharge, laser ablation, and electrochemical oxidation.[5] In bottom-up approaches, carbon dots are created by the application of harsh thermal treatments to small molecular precursors such as carbohydrate sugars, which allow rearrangement of carbon bonds to form larger conjugated structures.[5] These traditional methods all result in polydisperse fragments that require size fractionation to obtain specimens of the desired structural size range.[10] Due to the non-uniform nature of such carbonized fragments, the exact chemical structure of each carbon dot is not known, and reproducibility is variable.[9] Additionally, the quantum yields of carbon dots synthesized through the aforementioned conventional methods are commonly low, in the range of 1 to 3%,[10] due at least in part to structural defects that result from the synthetic methods. In furthering bottom-up approaches, there have been prominent efforts by the graphene research community in fabricating anatomically defined nanographene with precisely known structures from small molecules with various methods such as C-C bond forming reactions in solution-mediated chemical synthesis, surface assisted synthesis under ultra-high vacuum, and chemical vapor deposition among others.[11] Such efforts have led to the synthesis of small molecular-sized fragments of graphene

such as rylenes and cycloarene molecules,[12] curved fragments of fullerenes[13] and nanotubes,[14] and larger nanometer-sized structures such and graphene nanoribbons[15]. However, exceedingly few methods are yet available to precisely organize such molecules into homogeneous layers and particles.[16] While cyclophane skeletons have been exploited to organize polyaromatic hydrocarbons in stacks, they are synthetically challenging and have been structurally limited to two layers.[17]

Herein we test a novel bottom-up approach to assembly of aromatic carbon layers, using DNA-based synthesis to build luminescent carbon structures that mimic the properties of carbon dots. This approach offers several significant advantages over standard carbon dots, and over inorganic quantum dots in general. Perhaps most important, it offers complete structural control, as the DNA-carbon assemblies (DNA-CA) are built layer-by-layer. This results in monodisperse structures in which every component is defined with zero defects, and in which the electronic and optical properties are controlled and tunable.

a

	Quantum Yields	Size and structure control	Toxicity
DNA Carbon Assemblies (This work)	Varies, up to 29%	Precisely controlled	Low, carbon based
Carbon Dots (CD)/ Graphene Quantum Dots (GCD)	Generally low (1-3%)	Polydisperse with irregular molecular structure	Low, carbon based
Semiconductor Quantum Dots	Typically 1-10%, with cases exceeding 50%	Polydisperse with known structure	High, often contains Cd and Pb

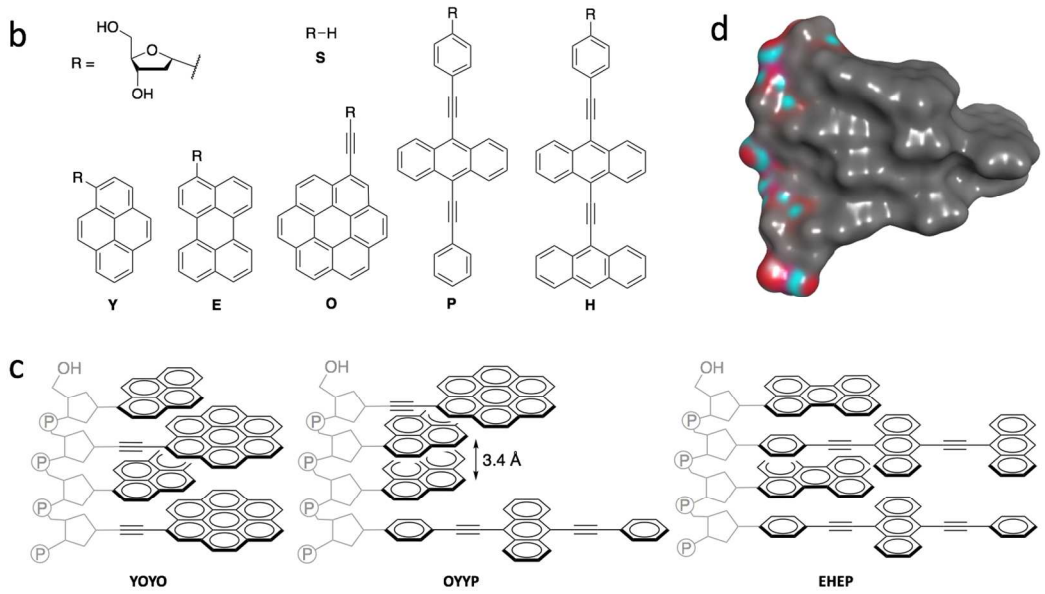

Figure 1. a) Comparison of DNA-based assemblies to carbon dots and semiconductor quantum dots. b) Structures and one-letter abbreviations of polyaromatic hydrocarbon moieties C-linked to deoxyribose monomer. c) Stucture of DNA- carbon assemblies with sequences 5'-YOYO-3', 5'-OYYP-3' and 5'-EHEP-3', held together by phosphate linked DNA backbone. d) Surface map model of DNA-based carbon dot mimic with sequence EHEP. Carbon atoms are depicted in gray, while phosphate and oxygen regions are in blue and red (Amber12 energy minimization).

Results

Design principles. Our design strategy for this work is to use the DNA backbone as a scaffold for assembling aromatic carbon fragments. The use of DNA as the basis for layered hydrocarbon assembly makes logical sense; the structure of DNA evolved to arrange the aromatic nucleobases in a stacked arrangement, with spacing of 3.4 Å,[18] which is the same as that in the lattice sheets of graphite[19], and the carbon sheet arrangements in carbon dots.[20] DNA can be assembled on an automated synthesizer unit-by-unit, adding successive aromatic structures (normally DNA bases) with precise control and high yield. By replacing DNA bases with aromatic hydrocarbons (fragments of graphene), we can use the DNA backbone as a scaffold to arrange individual aromatic species into a nanometer-sized stacked assembly, essentially homogeneous fragments of multilayer graphene. Just as DNA sequences can be varied during synthesis, the order and composition of layers of a carbon assembly could be varied to alter structure and properties.

Our goal in this work was to explore the range of luminescence properties achievable with assembled all-carbon chromophores, as homogeneous small models of stacked graphene. In previous work our laboratory has explored the assembly of fluorophores on a DNA backbone, and has investigated the applications of these composite assemblies in fluorescence imaging and sensing.[21-24] However, the earlier work involved chiefly heterocycle fluorophores, which

contain heteroatom components that can in some cases confer undesirable properties. For example, some N-nucleosides are chemically unstable because they have proton acceptor sites, and some fluorophores reported previously are nonplanar, potentially disrupting the stacking and electronic interactions between adjacent chromophores. To avoid these issues and explore graphite-like structural effects, in this new study we focused on an assembly system comprising only of stacked layers of planar polyaromatic hydrocarbon monomers. A few earlier studies have reported properties of assembled hydrocarbon fluorophores in DNA,[25-30] but those studies reported properties using only small numbers of combinations. Thus, emission properties were limited in diversity, and they were not tested for imaging. Therefore, in the present work we aimed to generate relatively large numbers of assemblies from a considerably more diverse set of component hydrocarbons.

The five synthetic DNA-like monomers comprising our novel DNA-carbon assemblies include pyrene (Y), perylene (E), coronene (O), which are direct fragments of graphene, and alkyne-linked anthracenes and bi-anthracenes (P and H) which are aromatic carbon structures known to provide excellent optical properties in light emitting displays,[31] and a non-fluorescent spacer molecule (S) (Figure 1b). These all-carbon polyaromatics are attached to deoxyribose in place of the DNA base, enabling them to be linked together to form an oligomer via the DNA phosphate backbone (Figure 1c,d). The anomeric orientations of these hydrocarbon bases are all the same configuration, allowing them the potential to align and closely stack as do DNA bases.

Monomer and Library synthesis.

Synthesis of the DNA-CA monomers involved the attachment of the polyaromatic hydrocarbon fragments to a deoxyribose derivative (Hoffer's chlorosugar) via varied C-C bond forming reactions such as Grignard cross-coupling,[32] and Sonogashira and Suzuki couplings (see Supporting Information (SI)). These monomers are converted into dimethoxytrityl-protected phosphoramidite derivatives for oligonucleotide synthesis with standard phosphoramidite chemistry. The collective absorption spectra of these monomers span from the UV to visible range, with Y and O dominating the UV region (350-400 nm) while E, P and H are strongly absorbing in the visible range (400-515 nm). In their emission spectra, Y and O are blue emitting, while E, P and H are cyan, green and yellow emitting (SI Figure S1).

Next, we employed the monomers in synthesis of a library of tetramer-length assemblies. Using standard combinatorial split-pool chemistry (see SI), we generated a library of 1296 tetrameric DNA-CA sequences on PEG-polystyrene beads (Tentagel, 130 μm) for the high

throughput screening of carbon dot-like properties. The method yields one compound per bead, allowing convenient differentiation of properties and sequences. The identity of each DNA-CA sequence was encoded by a chemical tagging approach based on acylcarbene chemistry, as originally developed by Still and modified by Schreiber.[33-34]

Library screening.

Visualization of the beads under a 365 nm excitation source revealed an array of individual emission colors ranging from blue to the far orange end of the visible spectrum (Figure 2a). In the library, new shades of blue, green, yellow and orange were observed – including redshifted emission hues not seen in any of the monomers. A machine vision algorithm (SI Figure S4) was written and employed for the rapid, automated screening of the RGB values of the emission colors from 1448 library beads, affording information on the overall color distribution (Figure 2e) and the brightness profile (Figure 2f) of the solid supported DNA-CAs in the library. The room temperature color distribution of our DNA-CAs profiled in the CIE chromaticity diagram suggest their potential utility in multiplex imaging and possibly even display applications (Figure 2e).[35-36] To screen for photobleaching resistance, the RGB brightness values of the library beads were monitored as the beads were exposed to 365 nm UV for 5 min increments in air (for a total of 20 min of exposure). This allowed us to locate and isolate the brightest, bleaching-resistant beads for the decoding of their corresponding DNA-CA sequences (Figure 2b). Interestingly, when excited at a longer wavelength (490 nm), many beads of the library displayed altered emission colors (Figures 2c, S5) - a phenomenon reminiscent of the excitation wavelength dependent emission of carbon

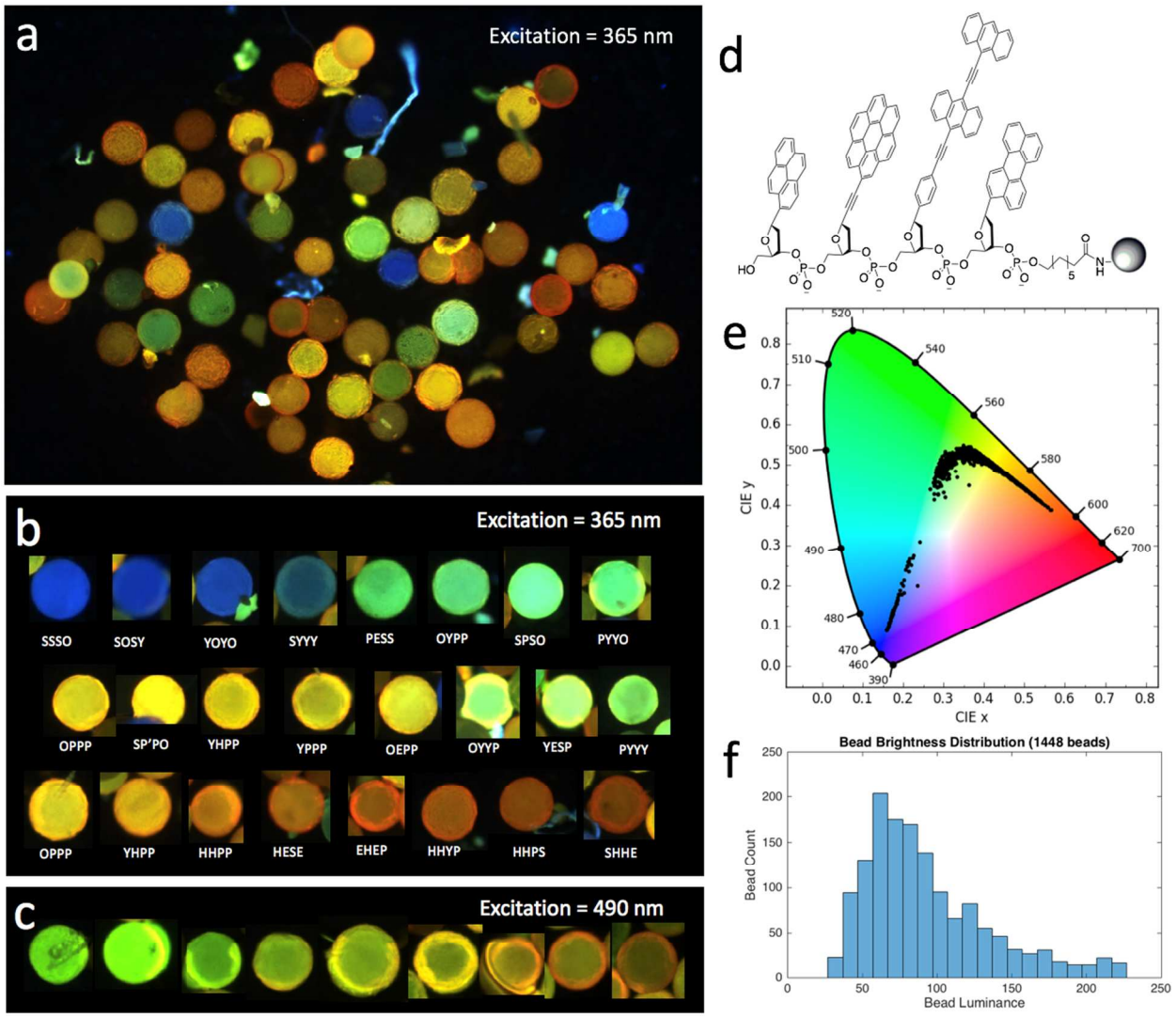

Figure 2. a) Epifluorescence image of random library beads, each carrying a unique DNA-CA sequence, excited at single wavelength (365 nm). Visible light emission of the solid supported DNA-CAs ranges from blue to deep orange. b) Selected library beads of varied emission colors (365 nm excitation) and their corresponding decoded sequence identities. c) Visible light emission of selected DNA-CA library beads at longer wavelength excitation (490 nm). d) Molecular structure of a DNA-CA sequence (YOHE) synthesized on PEG-polystyrene bead. e) CIE color profile of the visible light fluorescence of 1448 libary beads at 365 nm excitation. f) DNA-CA bead brightness distribution at 365 nm excitation.

dots.[5, 37] The library screening effort yielded a list of candidate DNA-CAs of varied emission colors that were predicted to have high photostability.

Synthesis and characterization of specific DNA-CAs. A set of solid-supported candidate DNA-CAs having the highest fluorescence brightness and photobleaching resistance was sorted into four broad color groups - blue, green, yellow, orange, and several sequences from each color group were chosen to be resynthesized in free, aqueous soluble form (Figure 3a). We found

that the water solubility of more hydrophobic DNA-CA sequences could be enhanced by the addition of phosphate containing spacer (S) units at the ends of the sequence. For example, the sequence EHEP could not be easily resolubilized in aqueous solution upon vacuum drying; the addition of helper spacers (5'-SSEHEPSS-3') resolved this issue. Solution studies (Figures 3c, S8a-b) showed that at lower concentrations the DNA-CAs remained in solution in primarily monomeric state, while at higher concentrations (which varied with sequence), aggregation was seen, a phenomenon well documented previously with other DNA-fluorophore assemblies.[38]

Although several among the resynthesized sequences exhibit gradual photobleaching (10 – 50 % loss of emission over 15 min) on prolonged UV exposure (365 nm) (Figure S10), we identified six DNA-CAs that undergo virtually no photobleaching in air-saturated solution (Figure 4), exhibiting unusually high photostability for organic fluorophores. Spectra taken over a 15-minute timespan are shown in Figure 4. The aqueous phase DNA-CAs are characterized by broad emission spectra across the visible range, having one to several emission peaks. For example, the emission of SPSO is a broad band spanning from 425 to 650 nm, with a single maximum at 500 nm, while PESS emits from 430 to 580 nm with two maxima at 445 and 465 nm. It was found that with increasing DNA-CA concentration, the peaks in aqueous phase emission spectra displayed broadening, redshifting, and change in intensities, which we attribute to DNA-CA clustering and aggregate formation in water (see SI Figure S16, S17). and Quantum yields of these DNA-CAs vary from modest (0.01) to relatively high (0.29). Long-wavelength absorption maxima vary from 342 to 550 nm, while lifetimes range from 1 ns to 42 ns (Figure 4). As a result of our library screening strategy, the selected DNA-CA sequences possess excellent photostability and brightness properties, showing almost no photobleaching on prolonged exposure to UV in air.

Dynamic light scattering experiments of the dilute (0.1 uM) aqueous phase DNA-CA SPSO reveal that they have highly uniform, almost monodisperse particle sizes of less than 1 nm (Figure 4c), consistent with a state that is monomeric or perhaps containing up to 2-3 monomers. At higher concentrations (10 μM) they were found to form low polydispersity aggregates of about 100 nm in size (SI Figure S8b).

We also tested the ability of DNA-CAs to remain fluorescent in a variety of environments, such as in a collagen hydrolysate hydrogel (Figure 3b), and in a polyurethane thick film dispersion on a flexible cellulose acetate substrate, which simulates the multichromatic emission from a UV-backlit semiconductor quantum dot display (Figure 3d). These tests of fluorescence in varied environments indicate that DNA-CAs could potentially have utility in diverse

applications such as dyes in fluorescence guided surgery[39] or emissive layers in organic light emitting displays.[40]

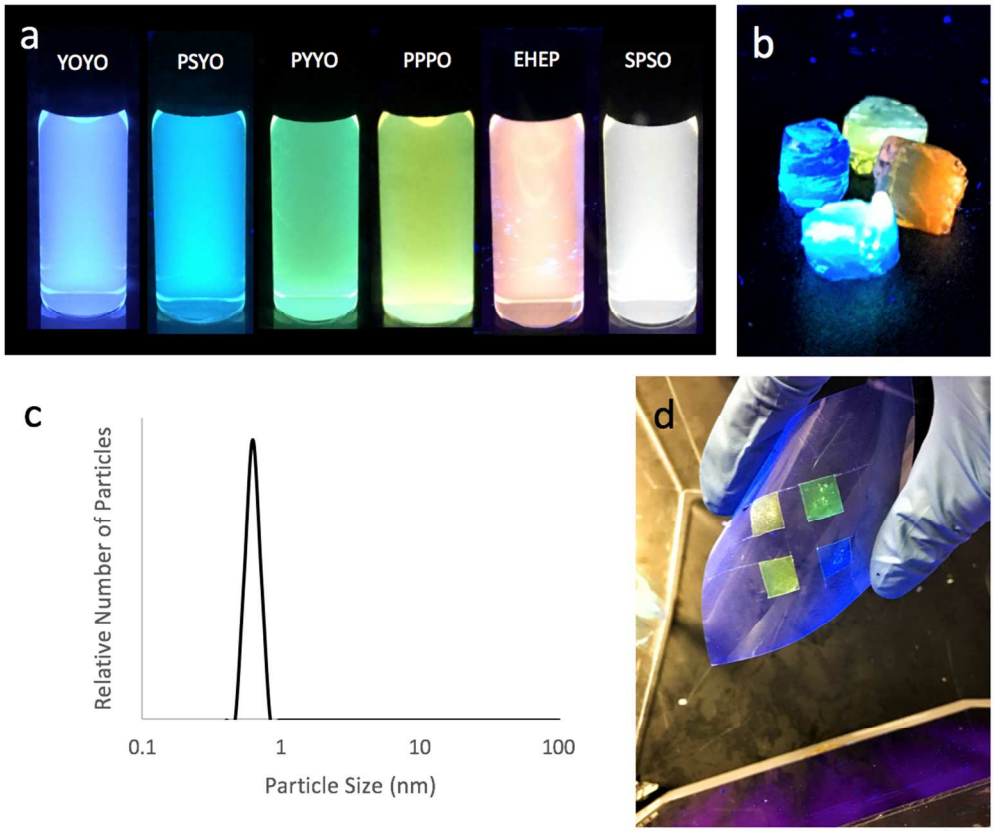

Figure 3. a) Aqueous phase DNA-based carbon dot mimics displaying a range of emission colors such as blue, green, yellow, orange, and white, at 365 nm excitation (10 μM). Sequence denoted in 5'->3'. b) Fluorescent DNA-CAs dispersed in collagen hydrolysate hydrogel, showing retention of fluorescence emission in more condensed media. c) Dynamic light scattering measurements of aqueous phase DNA-CA (0.1 μM SPSO) measurements show small particle sizes of <0.1 nm with low polydispersity. d) DNA-CAs dispersed in water-based polyurethane, screen-printed as thick film on flexible cellulose acetate sheet, excited by 365 nm backlight.

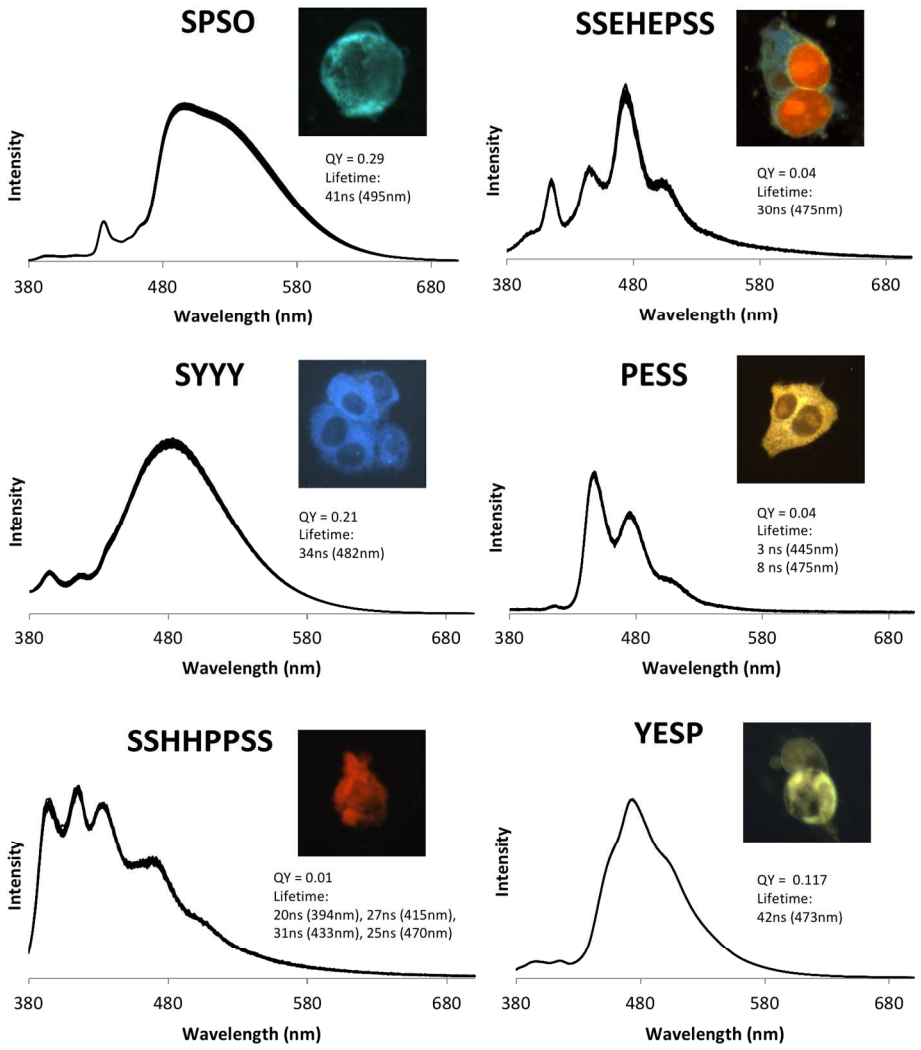

Figure 4. Optical properties of the DNA-CAs selected for bioimaging. Emission spectra of aqueous phase DNA-CAs were measured at 1 minute intervals over a period of 15 minutes of 365nm UV exposure, showing excellent resistance to photobleaching. Inset images show visible light emission of HeLa cells stained with individual pure DNA-CAs, excited with 365 nm UV.

Cell imaging experiments. Many bioimaging and biomedical applications of luminescent molecules and nanoparticles depend on their ability to be delivered into intact cells. To test this issue with DNA-CAs, we incubated live HeLa cells with a series of six selected oligomers that displayed exceptional photostability to UV exposure and diverse emission colors. For each staining experiment, cells were incubated in 20 µL phosphate-buffered saline (PBS) containing 0.1 to 1.0 mM DNA-CA solution, and were subsequently imaged by epifluorescence microscopy (Figures 4,5). The separately stained HeLa cells exhibited a multispectral range of fluorescence

spanning much of the visible spectrum – azure blue with SYYY, turquoise green with SPSO, banana yellow with YESP, lemon yellow with PESS, tangerine orange with SSEHEPSS, and amber orange with SSHHPPSS (Figure 4). High cellular uptake of the DNA-CAs led to their bright emission above that of the medium, permitting direct visualization of the cells without a washing step. Interestingly, the emission hues of certain DNA-CAs at these concentrations were environmentally dependent. For example, PESS exhibits green fluorescence in free solution, but yellow fluorescence in intact HeLa cells (Figures 4, S9), whereas SPSO appears white in free solution, but turquoise green in HeLa cells (Figures 4, S9).

The DNA-CAs tended to rapidly localize (< 5 min) in the cell cytoplasm without entering the nucleus (Figures 5a,c), with the exception of two sequences, SSEHEPSS (Figures 5f,g, S13), which showed apparent nuclear penetrating ability and a tendency to accumulate in subnuclear compartments (Figures 6e,f, S12A, S13). Interestingly, the emission color of SSEHEPSS appears to vary with its location within the cell – bright orange in the nucleus, and green-white in the cytoplasm (Fig. 6). A different sequence, PESS, was also found to produce emission in two colors in stained HeLa cells, green and yellow, depending on the degree of cell uptake (Fig. S14). When imaged at high resolution, the fluorescence of cytoplasm-localized SYYY had a punctate appearance, suggesting an endosomal uptake mechanism for DNA-CAs (Fig. S15). Clearly the uptake and localization behavior of these molecules depends on their sequence and possibly charge, and more work will be needed to elucidate the mechanisms involved.

For intracellular applications, we considered the possibility that that nucleases might potentially cleave the phosphodiester backbone of DNA-CAs, causing a change in fluorescent spectra as chromophore stacking is disrupted. To investigate the influence of cellular factors on the DNA-CA biostability, we incubated HeLa cells in DNA-CA containing media over a period of 3 h. Results show little toxicity of DNA-CAs to the cells, and the original photoluminescence properties were generally preserved, suggesting that the phosphodiester bonds are mostly stable under these conditions, although we cannot rule out some cleavage in the cases that show altered color in different compartments. We also found DNA-CAs suitable for tracking of cellular compartments such as secretory vesicles (Figure 5h).

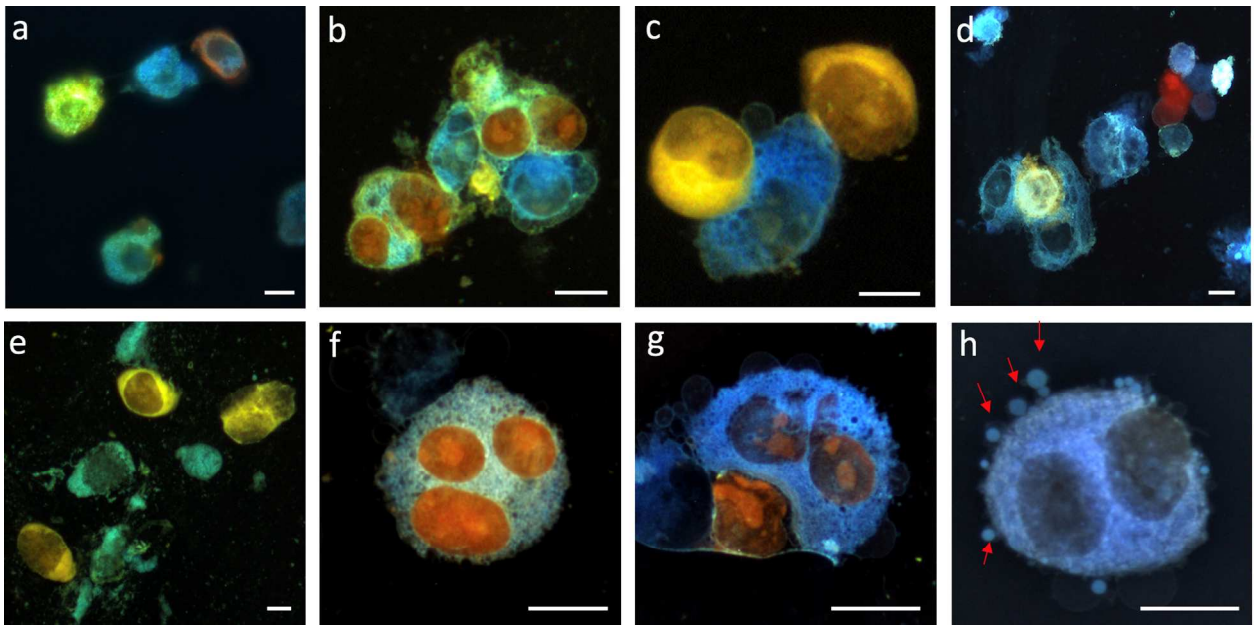

Figure 5. Epifluorescence images of DNA-CA stained live HeLa cells. a-f) Multichromatic emission at single wavelength excitation (365 nm). a) HeLa cells stained with SYYY (blue), YYYP (green), YESP (yellow green), SSHHPPSS (orange). b) SYYY (blue), SPSO (green), PESS (yellow), SSEHEPSS (orange). c) SYYY (blue) and PESS (yellow) d) PESS (yellow), SYYY (blue), YYYP (green) SSHHPPSS (orange-red). e) PESS (yellow) and SPSO (green). f) Single sequence SSEHEPSS stains HeLa cell nucleus orange and cell cytoplasm green-white. g) HeLa cell treated with SYYY(blue) and SSEHEPSS (orange). h) Blue fluorescence of SYYY seen in secretory vesicles migrating away from HeLa cell. Scale bars: 10 μm. In a-e, cells were stained separately with different dyes and then combined for the images. Note that images are single photographs without recombining false-colored images.

Discussion

Our experiments have shown that the assembly of hydrocarbon fluorophores in a DNA-like arrangement can result in a broad spectrum of fluorescence emission with a single short-wavelength excitation source. Importantly, these molecular assemblies can exhibit very high photostability; indeed, for several DNA-CA dyes we were unable to observe any photodegradation at all even after several minutes of UV irradiation in air (Fig. 4). This degree of stability is highly unusual for organic fluorophores, and offers a significant point of utility. We note that such hyper-stability was not observed in previous heteroatom-containing DNA fluorophores.[41] It should be noted that not all such hydrocarbon dyes in DNA are photostable; indeed, we recently described a dimeric alkynylpyrene dye that rapidly photoreacts, switching its emission from green to blue.[42] Despite having alkynyl groups similar to those alkynylpyrenes, the current sequences SPSO and SSHHPPSS remain completely unbleached under the same conditions. The origin of the photostability is likely sequence dependent, as several other resynthesized DNA-CAs containing the same monomers but in different arrangement are prone to photobleaching (SI Figure S10). The use of a library approach in the present case allowed us

to search through hundreds of sequences to identify particularly stable examples. Photostability is cited as an appealing feature of carbon dots in imaging,[43] and our new data establish that the current selected DNA-CAs can also exhibit this property.

A key property of DNA-CAs that distinguishes them from carbon dots is their discrete and homogeneous molecular structure. Their DNA-like oligomeric framework enables their rapid assembly using standard DNA synthesis chemistry; however, synthesis of the new hydrocarbon structures is even simpler than DNA synthesis because there are no amino groups (such as occur in DNA) that require protection and deprotection. The DNA backbone arranges the hydrocarbon layers so that they can potentially stack (like multilayer graphene) in the ground and/or excited states (see model in Fig. 1). It should be noted, however, that the structures are unlikely to be completely rigid, as the DNA backbone between chromophores has several rotatable bonds. We expect that dispersive and hydrophobic forces will likely cause the hydrocarbons in the assemblies to remain in a stacked configuration most of the time,[44] although more structural studies will be needed to confirm or refute this hypothesis. We also observe that, unsurprisingly, these amphiphilic molecules exhibit a clear concentration-dependent tendency to aggregate, likely driven by the need to reduce hydrophobic surface area. DLS experiments of one sequence (SPSO) show large soluble aggregates of 100 nm diameter at higher concentrations (1 μM), which are presumably in equilibrium with monomers or small aggregates of ~1 nm diameter seen at low concentration (0.1 μM). Similar aggregation has been observed before in other DNA-hydrocarbon molecules, and has been used to make ordered assemblies in the solid state.[41] Our tests with two sequences here (SSEHEPSS and SSHHPPSS) have shown that addition of charged monomers lacking hydrocarbon chromophores enhances solubility, and such strategies have been previously useful in reducing aggregation in DNA polyfluorophores when a monomeric state is desired.[45]

The defined molecular structure of individual DNA-CA dyes offers another significant advantage; namely, their amenability to bioconjugation and functionalization. They are in principle easily conjugatable to other molecules and species of interest, via known (and often commercially available) DNA conjugation methods.[46] Although this has not yet been proven for the current DNA-CAs, it has been shown previously that fluorescent DNAs can be conjugated to a single step to antibodies[46] and genetically encoded proteins.[47] Unlike typical graphene and semiconductor quantum dots, the current compounds are monovalent in their attachment, which can be made at either end of the DNA backbone.[41] In addition, DNA-CAs can be attached to DNA in trivial fashion, since they are already constructed on a DNA synthesizer.[47-48] This can potentially allow them to be used as labels for aptamers, or to be incorporated into larger DNA

assemblies such as origami and other nanostructures.[49] The chemical structure of DNA-CAs thus adopts the chemical versatility of DNA itself.

A major advantage of DNA-CAs over semiconductor and graphene quantum dots is that they are able to deliver long, redshifted emission wavelengths without the requirement of having larger nanometer-scale particle sizes. We find that when the oligomeric hydrocarbons are assembled into short, potentially stacked assemblies (i.e., dimers to tetramers), absorption properties reflect the combination of chromophores (ignoring hypochromicity and minor band broadening), while fluorescence is changed dramatically. We hypothesize that the red-shifted and broad fluorescence bands in DNA-CAs is caused by exciton coupling and the formation of excimers and exciplexes between the hydrocarbon components,[41] although more work will be needed to understand the photophysical behavior in detail.

These multichromatic DNA-CAs enable the simultaneous multicolor imaging of live cell structures with single wavelength excitation, without the need for multiple filter sets as is required by conventional dyes. Our DNA-CAs exhibit multicolor photoluminescence as do semiconductor quantum dots and carbon dots, with emission colors that span the visible spectrum, and with variable emission colors that depend on excitation wavelength. Although bioimaging demonstrations of carbon dots have difficulty capturing more than one emission color within the same image, requiring multiple combined images to demonstrate multicolor emission, this is not an issue with the current DNA-CAs, which we have shown can readily stain cells with multiple emission colors within the same image. Unlike semiconductor quantum dots which have narrow emission bands,[50] but similar to carbon quantum dots,[2, 5] the current DNA-CAs exhibit broad absorption and emission spectra (width of emission band spans 100 – 150 nm). The broad emission spectra of DNA-CAs would result in significant overlapping of spectral signals if two or more DNA-CAs are used for multiplexed imaging. We expect that this issue can potentially be overcome by the use of spectral unmixing techniques[36, 51] to finely resolve localized DNA-CAs, or by the use of fluorescence lifetime imaging methods[52] to distinguish between sequences.

Interestingly, we have identified four DNA-CAs that exhibit near-white emission when in aqueous solution – SPSO (CIE coordinates 0.30, 0.33), PSYO (0.29, 0.33), PYYY (0.30, 0.33), YESP (0.30,0.33). These dyes have CIE chromaticity coordinates values close to the ideal white coordinate of (0.33,0.33).[53] There has been significant interest in development of molecular white-emitting dyes in the recent literature.[54-57] With consideration of DNA-CA photostability, these luminescent assemblies could potentially be applied in white organic light-emitting devices or sensors.[58] Interestingly, our cell staining experiments show that two of these

dyes (SPSO and YESP) shift their emission away from white when incorporated into cells (Figure 4). The loss of white emission might be explained by the change in molecular environment surrounding the fluorophores, or by cellularly localized phosphodiesterase activity. We have documented in previous studies that some examples of fluorophores stacked on a DNA backbone exhibit variable emission colors depending on the environment, and have exploited such color change effects for use in analyte sensing.[21-23, 59]

The present DNA-carbon assemblies exhibit many of the desirable properties of semiconductor and graphene quantum dots,[60] including: (a) multispectral emission with UV excitation; (b) variable emission with changing excitation wavelength; (c) red shifting with increasing monomer size; (d) excited states that are delocalized throughout the structure; (e) a range of fluorescence lifetimes; (f) strong resistance to photobleaching; and (g) bright fluorescence. Moreover, our monomer-by-monomer assembly strategy allows the control of multilayer carbon structure in a way that has not been achievable to date. Unlike ablative nanomaterials that suffer from poor reproducibility in synthesis, DNA-CAs offer complete molecular reproducibility, and are constructed in thousands of tunable variations.

Conclusion

In conclusion, we have demonstrated a novel DNA-based approach to assembling polyaromatic hydrocarbon fragments in a precise manner, in a bottom up synthesis quite distinct from current carbon dot synthesis. Our DNA-carbon assemblies have precisely known molecular structures and exhibit many of the properties of carbon dots. They display multispectral emission at single excitation, with selected sequences having exceptional photostability. In tests of their utility, we have exploited their multicolor luminescence in the bioimaging of live cells. We envision future designs of DNA-CAs with interesting properties that can be readily constructed by the inclusion of other hydrocarbon monomers. The prospect of assembling larger graphene fragments[61] by this approach is intriguing, and remains to be tested. Our system provides a promising method to construct structurally uniform carbon assemblies, and may inform the graphene research field in general.

Experimental Methods

Chemicals and reagents. Solvents and reagents for DNA-CA monomer synthesis were purchased from Sigma-Aldrich, Merck Millipore, TCI America, Alfa Aesar, Combiblocks, Praxair, ArkPharm and Fisher Scientific. DNA synthesis reagents were purchased from Glen Research

and Merck Millipore. All reactions were conducted under argon atmosphere unless otherwise noted. Merck 60Å 200-425 mesh silica gel was used for column chromatography.

General Instrumentation. ^{1}H and ^{13}C NMR spectra were measured with Varian NMR spectrometers (Inova 300, Varian 400 and Mercury 400). For optical spectra, DNA-CAs were prepared as ~1 μM solutions in water (Molecular Biology Grade, Corning). Absorption spectra were measured with Cary 100 Bio UV-Vis spectrometer, fluorescence spectra obtained by Jobin Yvon-Spex Fluorolog 3 spectrometer, and fluorescence lifetime measurements were made with a PTI EasyLife LS spectrometer. Mass spectra were obtained using ESI or MALDI-TOF ionization modes at the Stanford University Mass Spectrometry Facility. HPLC was performed with a Shimadzu LC-20AD equipped with SPD-M20A diode array detector and Phenomenex Jupiter reverse phase C5 column. Dynamic light scattering measurements were made with a Malvern Instruments Nanoseries ZS90 Zetasizer. Epifluorescence microscopy for cell bioimaging and library screening were conducted on a Nikon Eclipse 80i microscope equipped with Nikon Plan Fluor 4x – 40x objective, and QIClick digital CCD camera, with a high pressure 100W high pressure mercury lamp as the excitation source (365 nm mercury plasma emission line), 340-380 nm excitation filter and > 420 nm long-pass emission filter. Photographs of aqueous phase DNA-CAs, DNA-CAs in hydrogel and flexible DNA-CA display were captured with an iPhone 6S+ camera, with a 365 nm gel transilluminator UV source (VWR LM-20E) as backlight.

DNA-CA library construction. The DNA-CA library was synthesized on amine-functionalized polyethylene glycol coated polystyrene beads (Merck NovaSyn TG amino resin, 130 μm diameter) using a previously reported protocol.[62] The surface of each bead carries a unique DNA-CA sequence, attached via a 10-hydroxy-decanoic acid linker to the amino moiety of the bead, along with a cleavable low molecular weight binary chemical tag that uniquely identifies the DNA-CA sequence.[33, 63] In total, the library contained a theoretical 1296 unique DNA-CAs sequences. Overall average stepwise coupling yield for the library tetrameric DNA-CA sequences was 95%. After library synthesis, the DNA-CAs were deprotected with 50 mM potassium carbonate in methanol, washed with EDTA in DMF, water, acetonitrile, DCM and dried under argon gas stream.

Library screening procedure. Library beads were adhered to a double-sided tape attached to a microscope slide, clustered in zones containing about 20-30 beads each (Figure 2 shows an image of a zone). The attached beads on each slide were moistened with 200 µL water for 5 minutes before each visualization under epifluorescence microscope with a 365 nm excitation source. Images of the fluorescent beads in each zone were captured and fed into a custom machine vision-based bead detector program (Figure 3), which extracts the RGB values, luminosity value, and position of each bead. The code for this program is provided in a separate document. To select for photostability, approximately 2000 beads were tracked over a period of four days, with a 5-minute exposure to 365 nm UV per day. At the end of the four day period, beads exhibiting highest brightness and photostability were selected, and sequenced by decoding of the cleavable tags. For DNA-CA sequence decoding, single beads were submerged in 3 µL of CAN solution (0.5 M ceric ammonium nitrate in water:acetonitrile 1:1) and 3 µL decane in a sealed capillary tube as described.[33] The capillary tube was sonicated for 3 hours, centrifuged, and the organic decane layer containing cleaved tags were derivatized with N,O-Bis(trimethylsilyl)acetamide and analyzed with GC-ECD following the literature procedure.[33]

Resynthesis and characterization of high brightness and photostable DNA-CA sequences. Selected high-brightness and high-photostability DNA-CA sequences from the library screening effort were resynthesized via standard oligonucleotide synthesis on an ABI 394 DNA synthesizer. The DNA-CA tetramers were synthesized at 1 µmol scale on 3'-phosphate CPG columns (Glen Research), deprotected with 50 mM potassium carbonate in methanol, preparatory HPLC purified with a C5 reverse phase column, using pH 7.0 adjusted 50 mM triethylammonium acetate buffer and acetonitrile as eluents. The purified sequences were dried by vacuum concentrator, reconstituted in molecular biology grade water, characterized by MALDI-TOF mass spectrometry, and optical properties measured.

Flexible DNA-CA display fabrication. 0.1 µmol of each DNA-CA was mixed with 20 µmol Varathane water-based polyurethane and screen-printed on flexible cellulose acetate substrate and left to air dry. The emissive display was pumped with a 365 nm UV backlight (gel transilluminator) for imaging.

DNA-CA-containing collagen hydrolysate hydrogel synthesis. To create hydrogel solutions, 3 g dextrose was mixed with 0.5 g collagen hydrolysate powder in 10 mL water. The suspension was allowed to stand for 20 minutes, and then heated in a microwave oven until all solids were dissolved. 0.1 μmol of each DNA-CA was mixed with 100 μL melted hydrogel solution and left to set in plastic molds at 5 °C. The emissive hydrogel was excited with a 365 nm UV backlight (gel transilluminator) for imaging.

Cell culture and imaging studies. HeLa and HEK293T cells were seeded at a concentration of 3 × 10^4 cells per well to 96-well plate in supplemented DMEM culture medium (10% FBS, Gibco, Penicillin Streptomycin, Thermo Fisher Scientific) and incubated for 16 h at 37°C and 5% CO_2 with 95% humidity. Old medium was removed and cells washed once with 1xPBS pH 7.4 (Gibco). To detach cells, 20 μL of 0.25% Trypsin (Gibco) was added and incubated for 5 minutes at 37°C and 5% CO_2 with 95% humidity. Cells in each well were suspended in 50 μL fresh DMEM supplemented medium, and collected for centrifugation (3 mins, 800 RCF) at room temperature, the supernatant was discarded and cells resuspended in 20 μL fresh DMEM medium lacking phenol red (Gibco). A suspension of live cells was incubated with various DNA-CA dyes at 0.1 to 3 μM concentrations from 5 min up to 3 h for bioimaging. Cells were also incubated with 0.1% aqueous methyl green to visualize cell nuclei. Visualization and imaging of cells was carried out under an epifluorescence microscope at room temperature.

Acknowledgement. We thank the U.S. National Institutes of Health (GM106067, CA217809) and the U.S. Army Research Office (W911NF-13-1-0181) for support.

Supporting Information Available. Detailed methods, spectra, and characterization data. An additional supporting file contains code for the bead sorting and analysis software.

References

1. Wick, P.; Louw-Gaume, A. E.; Kucki, M.; Krug, H. F.; Kostarelos, K.; Fadeel, B.; Dawson, K. A.; Salvati, A.; Vázquez, E.; Ballerini, L.; Tretiach, M.; Benfenati, F.; Flahaut, E.; Gauthier, L.; Prato, M.; Bianco, A., *Angew. Chem., Int. Ed.* **2014,** *53*, 7714-7718.
2. Cao, L.; Meziani, M. J.; Sahu, S.; Sun, Y.-P., *Acc. Chem. Res.* **2013,** *46*, 171-180.
3. Castro Neto, A. H.; Guinea, F.; Peres, N. M. R.; Novoselov, K. S.; Geim, A. K., *Rev. Mod. Phys.* **2009,** *81*, 109-162.
4. Shen, J.; Zhu, Y.; Yang, X.; Li, C., *Chem. Commun. (Cambridge, U.K.)* **2012,** *48*, 3686-3699.

5. Lim, S. Y.; Shen, W.; Gao, Z., *Chem. Soc. Rev.* **2015,** *44*, 362-381.
6. Wang, H.; Zhang, Q.; Chu, X.; Chen, T.; Ge, J.; Yu, R., *Angew. Chem., Int. Ed.* **2011,** *50*, 7065-7069.
7. Wang, Z.; Ge, Z.; Zheng, X.; Chen, N.; Peng, C.; Fan, C.; Huang, Q., *Nanoscale* **2012,** *4*, 394-399.
8. Li, L.; Wu, G.; Yang, G.; Peng, J.; Zhao, J.; Zhu, J.-J., *Nanoscale* **2013,** *5*, 4015-4039.
9. Zhou, S.; Xu, H.; Gan, W.; Yuan, Q., *RSC Adv.* **2016,** *6*, 110775-110788.
10. Ray, S. C.; Saha, A.; Jana, N. R.; Sarkar, R., *J. Phys. Chem. C* **2009,** *113*, 18546-18551.
11. Narita, A.; Wang, X.-Y.; Feng, X.; Müllen, K., *Chem. Soc. Rev.* **2015,** *44*, 6616-6643.
12. Müllen, K., *ACS Nano* **2014,** *8*, 6531-6541.
13. Scott, L. T.; Jackson, E. A.; Zhang, Q.; Steinberg, B. D.; Bancu, M.; Li, B., *J. Am. Chem. Soc.* **2012,** *134*, 107-110.
14. Steinberg, B. D.; Scott, L. T., *Angew. Chem., Int. Ed.* **2009,** *48*, 5400-5402.
15. Cai, J.; Ruffieux, P.; Jaafar, R.; Bieri, M.; Braun, T.; Blankenburg, S.; Muoth, M.; Seitsonen, A. P.; Saleh, M.; Feng, X.; Müllen, K.; Fasel, R., *Nature* **2010,** *466*, 470-473.
16. Liu, R.; Wu, D.; Feng, X.; Müllen, K., *J. Am. Chem. Soc.* **2011,** *133*, 15221-15223.
17. Ghasemabadi, P. G.; Yao, T.; Bodwell, G. J., *Chem. Soc. Rev.* **2015,** *44*, 6494-6518.
18. Watson, J. D.; Crick, F. H. C., *Nature* **1953,** *171*, 737-738.
19. Bernal, J., *Proc. R. Soc. A* **1924,** *106*, 749-773.
20. Qu, S.; Wang, X.; Lu, Q.; Liu, X.; Wang, L., *Angew. Chem., Int. Ed.* **2012,** *124*, 12381-12384.
21. Kwon, H.; Jiang, W.; Kool, E. T., *Chem. Sci.* **2015,** *6*, 2575-2583.
22. Yuen, L. H.; Franzini, R. M.; Tan, S. S.; Kool, E. T., *J. Am. Chem. Soc.* **2014,** *136*, 14576-14582.
23. Jiang, W.; Wang, S.; Yuen, L. H.; Kwon, H.; Ono, T.; Kool, E. T., *Chem. Sci.* **2013,** *4*, 3184-3190.
24. Wang, S.; Guo, J.; Ono, T.; Kool, E. T., *Angew. Chem., Int. Ed.* **2012,** *51*, 7176-7180.
25. Malinovskii, V. L.; Wenger, D.; Haner, R., *Chem. Soc. Rev.* **2010,** *39*, 410-422.
26. Adeyemi, O. O.; Malinovskii, V. L.; Biner, S. M.; Calzaferri, G.; Haner, R., *Chem. Commun. (Cambridge, U.K.)* **2012,** *48*, 9589-9591.
27. Wojciechowski, F.; Lietard, J.; Leumann, C. J., *Org. Lett.* **2012,** *14*, 5176-5179.
28. Lindegaard, D.; Madsen, A. S.; Astakhova, I. V.; Malakhov, A. D.; Babu, B. R.; Korshun, V. A.; Wengel, J., *Bioorg. Med. Chem.* **2008,** *16*, 94-99.
29. Wilson, J. N.; Gao, J.; Kool, E. T., *Tetrahedron* **2007,** *63*, 3427-3433.
30. Teo, Y. N.; Kool, E. T., *Bioconjugate Chem.* **2009,** *20*, 2371-2380.
31. Huang, J.; Su, J.-H.; Tian, H., *J. Mater. Chem.* **2012,** *22*, 10977-10989.
32. Hocek, M.; Pohl, R.; Klepetářová, B., *Eur. J. Org. Chem.* **2005,** *2005*, 4525-4528.
33. Nestler, H. P.; Bartlett, P. A.; Still, W. C., *J. Org. Chem.* **1994,** *59*, 4723-4724.
34. Blackwell, H. E.; Pérez, L.; Stavenger, R. A.; Tallarico, J. A.; Cope Eatough, E.; Foley, M. A.; Schreiber, S. L., *Chem. Biol.* **2001,** *8*, 1167-1182.
35. Mueller-Mach, R.; Mueller, G. O., *Proc. SPIE* **2000,** *3938*, 30.
36. Strack, R., *Nat. Methods* **2016,** *13*, 35-35.
37. Cushing, S. K.; Li, M.; Huang, F.; Wu, N., *ACS Nano* **2014,** *8*, 1002-1013.
38. Cuppoletti, A.; Cho, Y.; Park, J.-S.; Strässler, C.; Kool, E. T., *Bioconjugate Chem.* **2005,** *16*, 528-534.
39. Nguyen, Q. T.; Tsien, R. Y., *Nat. Rev. Cancer* **2013,** *13*, 653-662.
40. Frecker, T.; Bailey, D.; Arzeta-Ferrer, X.; McBride, J.; Rosenthal, S. J., *ECS J. Solid State Sci. Technol.* **2016,** *5*, R3019-R3031.
41. Teo, Y. N.; Kool, E. T., *Chem. Rev.* **2012,** *112*, 4221-4245.
42. Chan, K. M.; Kölmel, D. K.; Wang, S.; Kool, E. T., *Angew. Chem., Int. Ed.* **2017,** *56*, 6497-6501.
43. Wang, W.; Damm, C.; Walter, J.; Nacken, T. J.; Peukert, W., *Phys. Chem. Chem. Phys.* **2016,** *18*, 466-475.
44. Guckian, K. M.; Schweitzer, B. A.; Ren, R. X. F.; Sheils, C. J.; Tahmassebi, D. C.; Kool, E. T., *J. Am. Chem. Soc.* **2000,** *122*, 2213-2222.
45. Teo, Y. N.; Wilson, J. N.; Kool, E. T., *J. Am. Chem. Soc.* **2009,** *131*, 3923-3933.

46. Guo, J.; Wang, S.; Dai, N.; Teo, Y. N.; Kool, E. T., *Proc. Natl. Acad. Sci. U.S.A.* **2011,** *108*, 3493-3498.
47. Singh, V.; Wang, S.; Kool, E. T., *J. Am. Chem. Soc.* **2013,** *135*, 6184-6191.
48. Clark, S. A.; Singh, V.; Vega Mendoza, D.; Margolin, W.; Kool, E. T., *Bioconjugate Chem.* **2016,** *27*, 2839-2843.
49. Deng, Z.; Samanta, A.; Nangreave, J.; Yan, H.; Liu, Y., *J. Am. Chem. Soc.* **2012,** *134*, 17424-17427.
50. Rizvi, S. B.; Ghaderi, S.; Keshtgar, M.; Seifalian, A. M., *Nano Rev.* **2010,** *1*.
51. Vonesch, C.; Aguet, F.; Vonesch, J. L.; Unser, M., *IEEE Signal Process. Mag.* **2006,** *23*, 20-31.
52. Berezin, M. Y.; Achilefu, S., *Chem. Rev.* **2010,** *110*, 2641-2684.
53. Kamtekar, K. T.; Monkman, A. P.; Bryce, M. R., *Adv. Mater.* **2010,** *22*, 572-582.
54. Xu, B.; Wu, H.; Chen, J.; Yang, Z.; Yang, Z.; Wu, Y.-C.; Zhang, Y.; Jin, C.; Lu, P.-Y.; Chi, Z.; Liu, S.; Xu, J.; Aldred, M., *Chem. Sci.* **2017,** *8*, 1909-1914.
55. Varghese, R.; Wagenknecht, H.-A., *Chem. Eur. J.* **2009,** *15*, 9307-9310.
56. Park, S.; Kwon, J. E.; Kim, S. H.; Seo, J.; Chung, K.; Park, S.-Y.; Jang, D.-J.; Medina, B. M.; Gierschner, J.; Park, S. Y., *J. Am. Chem. Soc.* **2009,** *131*, 14043-14049.
57. Arcudi, F.; Đorđević, L.; Prato, M., *Angew. Chem., Int. Ed.* **2017,** *56*, 4170-4173.
58. Reineke, S.; Thomschke, M.; Lüssem, B.; Leo, K., *Rev. Mod. Phys.* **2013,** *85*, 1245-1293.
59. Kwon, H.; Chan, K. M.; Kool, E. T., *Org. Biomol. Chem.* **2017,** *15*, 1801-1809.
60. Song, Y.; Zhu, S.; Yang, B., *RSC Adv.* **2014,** *4*, 27184-27200.
61. Beser, U.; Kastler, M.; Maghsoumi, A.; Wagner, M.; Castiglioni, C.; Tommasini, M.; Narita, A.; Feng, X.; Müllen, K., *J. Am. Chem. Soc.* **2016,** *138*, 4322-4325.
62. Gao, J.; Strässler, C.; Tahmassebi, D.; Kool, E. T., *J. Am. Chem. Soc.* **2002,** *124*, 11590-11591.
63. Ohlmeyer, M. H.; Swanson, R. N.; Dillard, L. W.; Reader, J. C.; Asouline, G.; Kobayashi, R.; Wigler, M.; Still, W. C., *Proc. Natl. Acad. Sci. U.S.A.* **1993,** *90*, 10922-10926.

Graphical abstract

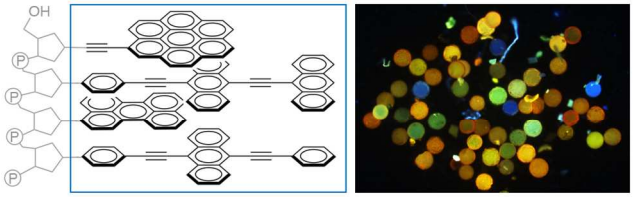

All-carbon polyaromatic assembly

Multichromatic emission with single wavelength excitation